Plasma chemistry and dust-particle generation in pure methane plasma: Influence of the RF electrode cleanliness

Isabelle Géraud-Grenier, Maxime Mikikian, Francois Faubert, Véronique Massereau-Guilbaud

Journal of Applied Physics ARTICLE scitation.org/journal/jap

Plasma chemistry and dust-particle generation in pure methane plasma: Influence of the RF electrode cleanliness

Cite as: J. Appl. Phys. **126**, 063301 (2019); doi: 10.1063/1.5099326
Submitted: 9 April 2019 · Accepted: 16 July 2019 ·
Published Online: 8 August 2019

I. Géraud-Grenier,[1] M. Mikikian,[2] F. Faubert,[1] and V. Massereau-Guilbaud[1]

AFFILIATIONS

[1]Groupe de Recherches sur l'Energétique des Milieux Ionisés (GREMI), UMR 7344 CNRS/Université d'Orléans, Site de l'IUT de Bourges, 63 avenue de Lattre de Tassigny, 18020 Bourges Cedex, France
[2]Groupe de Recherches sur l'Energétique des Milieux Ionisés (GREMI), UMR 7344 CNRS/Université d'Orléans, 14 rue d'Issoudun, 45067 Orléans Cedex 2, France

ABSTRACT

Hydrocarbon dust-particles are formed and grown to a large size (around 1 μm) in a low pressure capacitively coupled radio frequency discharge in methane. The methane decomposition leads to the formation of both spherical dust-particles in the plasma bulk and coating on the electrodes. Under ion bombardment, the coating on the biased top electrode peels off, leading to the fall of flakes. To better understand the role played by the electrode surface state on the plasma chemistry and on the dust-particle growth, experiments are carried out in two different initial conditions for the electrodes: (i) without any coating and (ii) with a homogeneous hydrocarbon coating. Spherical dust-particle growth is followed using the temporal evolution of the DC self-bias voltage. At the end of the experiment, dust-particles and flakes are collected and observed by scanning electron microscopy. Using mass spectrometry, temporal evolutions of neutrals, ionic species, and positive ion energies are investigated. Between the two experimental conditions, no strong differences were observed on the plasma chemistry. However, the self-bias voltage is strongly modified as well as the dust-particle growth and dynamics.

I. INTRODUCTION

Dusty plasma is composed not only of electrons, ions, neutral gas atoms, and molecules but also of charged dust-particles that may be as large as a few micrometers. Since Langmuir *et al.*[1] discovered dust-particles in glow discharges, a lot of studies have been carried out in order to understand the mechanisms involved in dust-particle formation. While for microelectronic applications[2,3] the main objective is to avoid dust formation, dusty plasmas can be interesting in many other application fields where the incorporation of dust-particles in coatings enhances material or layer properties.[4,5] Dust-particles are also of high interest in astrophysics as they play an important role in several key phenomena.[6–8] For these reasons, a better understanding of the formation mechanisms of dust-particles in plasmas is of primary importance. Indeed, due to their electrical charging,[9] dust-particles strongly affect the plasma characteristics,[10] leading in certain conditions to complex plasma instabilities.[11,12]

Laboratory hydrocarbon dusty plasmas are frequently produced in chemically reactive gas mixtures like C_2H_2, C_2H_2-Ar, CH_4, or HMDSO-Ar.[13–22] While cyclic production/disappearance of dust-particles is easily observed in C_2H_2 or HMDSO-Ar,[14,18,22] in pure CH_4 plasmas, only one dust-particle generation is usually observed.[23]

In this work, dust-particle formation is initiated by the plasma-enhanced chemical vapor deposition (PECVD) technique in a pure methane radio frequency (RF) plasma. The methane decomposition leads to the formation of both an amorphous hydrocarbon thin film on the electrodes and of white spherical dust-particles growing in the gas phase. An additional component can be observed in the plasma, i.e., flakes coming from the spalling of the grown hydrocarbon thin film on the biased electrode. While the produced spherical dust-particles grow, they become negatively charged and are submitted to forces that keep them in levitation in clouds near the electrodes. The formation, trapping, and disappearance of dust-particles from the cloud under the RF electrode can be followed by measuring the DC self-bias voltage.

In order to reveal the influence of the electrode contamination on the dusty plasma chemistry and the dust-particle growth, experiments are performed in two different initial conditions for the

electrodes: (i) without any coating and (ii) with a homogeneous hydrocarbon coating.

Mass spectrometry (MS) has been used to investigate the temporal evolution of potential precursors and chemical species (neutrals and ions) involved in dust-particle growth. The temporal evolution of the mean energy of the positive ions is also determined and compared to the DC self-bias voltage. Dust-particles are collected at the end of the experiments. Their surface state is observed using scanning electron microscopy (SEM), and their diameter is determined. This paper is organized as follows: in Sec. II, the experimental setup and diagnostics are detailed. In Secs. III and IV, experimental results concerning the plasma chemistry and dust-particle growth kinetics are presented and discussed. A correlation between the different results is performed in order to underline the influence of the RF electrode cleanliness on the dust-particle formation. Finally, a conclusion section outlines the main results issued from this work.

II. EXPERIMENTAL SETUP AND PROTOCOL

The experimental setup is a classical capacitively coupled parallel plate RF reactor (Fig. 1) described in detail in a previous paper.[24]

The reactor is 56 cm in diameter and 48 cm in height and is pumped down to a residual pressure around 10^{-4} Pa. Within the chamber, a 13.5 cm diameter RF electrode is at the top and a 20 cm diameter grounded electrode is at the bottom. Aluminum electrodes are located 2.5 cm away from each other and are not cooled. The temperature of each electrode, measured using thermocouples, increases linearly during an experiment. For a fixed experiment of 20 min, the increase in temperature is of 20 K for the RF electrode and 7 K for the grounded one. Due to the asymmetry between the powered and grounded areas in the reactor, to the capacitively coupled system and to the large difference in ion and electron mobilities, a negative DC self-bias voltage (V_{DC}) is induced on the powered electrode with respect to the ground, in order to equalize ion and electron fluxes to the electrodes.[25] The time evolution of V_{DC} is recorded by an oscilloscope (Tektronix DPO 5034).

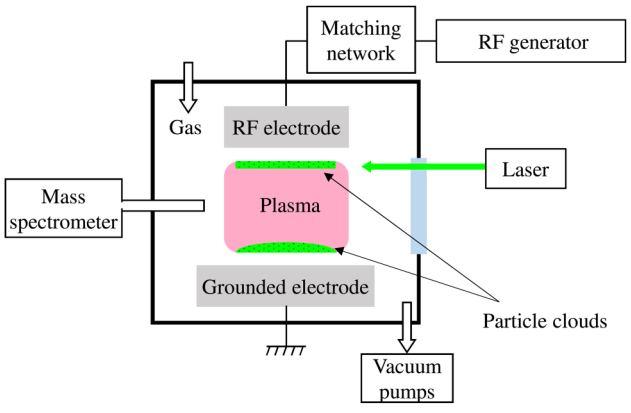

FIG. 1. Experimental setup.

Dust-particles are produced thanks to CH_4 at a working pressure of 120 Pa using a flow rate of 5.6 sccm (9.45×10^{-3} Pa m^3/s). An incident power of 80 W is delivered by a 13.56 MHz RF generator (Huttinger, PFG 300), through a matching network (Huttinger, PFM 1500 A).

As the plasma is well confined between the two electrodes and as the reactor walls are relatively far from this active region, no coating is deposited on the grounded reactor walls. However, a few particles are ejected from the plasma core and fall onto the reactor bottom.

Growing dust-particles are monitored by laser light scattering (LLS), using an Ar^+ laser at $\lambda = 514.5$ nm (Coherent, Innova 70 Spectrum). The laser beam is directed through the reactor parallel to the electrodes to observe dust-particle clouds. The scattered light and plasma emission are recorded with a digital camera (Sony, DSC-HX50) at a frame rate of 50 frames per second. At the end of some experiments, the reactor is opened, and dust-particles that have fallen on the grounded electrode are collected. Dust-particle morphology and size are analyzed using SEM.

The plasma chemistry is analyzed by mass spectrometry with a Hiden Analytical EQP 1000 device. Ionic and neutral species are sampled by the mass spectrometer through a 50 μm diameter orifice placed 1 cm outside the plasma and midway between the two electrodes. The residual pressure in the mass spectrometer is 1.2×10^{-6} Pa, and the pressure increases up to 4.8×10^{-4} Pa during the experimental process for a plasma chamber pressure of 120 Pa. The energy of the electron beam for neutral ionization is fixed at 70 eV.

To clarify the influence of the electrode cleanliness on the plasma chemistry and dust-particle generation, a precise experimental protocol has been elaborated to keep fixed discharge conditions (CH_4 at 120 Pa, 80 W, for 20 min):

1. The vacuum chamber is totally cleaned with sand paper and ethanol to remove the coating and the fallen dust-particles from the electrodes. The chamber is pumped down to 10^{-4} Pa during around 5 h.
2. First experiment (without coating): dust-particles grow and a coating is progressively formed on the electrodes. At the end of the experiment, a thin hydrocarbon film (around 1 μm) is deposited on the RF electrode and dust-particles have fallen onto the grounded electrode.
3. The reactor is not opened and is pumped down to 10^{-4} Pa until the powered electrode temperature cools down to the room temperature.
4. Second experiment of dust-particle growth (with coating).

III. DUST-PARTICLE BEHAVIOR

Electron impact decomposition of the CH_4 feed gas induces the formation of light species like atoms and molecules, radicals, and ions.[26] For the given experimental conditions, these species contribute to a spontaneous dust-particle generation. Different scenarios of dust-particle formation and growth have been proposed in various chemistries[11,27–30] and may be summarized as follows: a molecular growth process ends up with the nucleation and coagulation phase of nanometer-sized dust-particles. At the end of this

phase, the plasma contains permanently negatively charged dust-particles with a diameter of 20–50 nm. In low pressure discharges, dust-particles become negatively charged because of the high electron mobility compared to the heavy ions.[31] Under our typical experimental conditions, a dust-particle of 1 μm in diameter acquires a negative charge of 10^3 elementary charges according to Pandey *et al.*[32] Once these nanometer-sized dust-particles are formed, they continue to grow by surface deposition, i.e., by sticking of radicals and/or ions, which are created in the plasma bulk. At the same time, thin hydrocarbon films are deposited on both electrodes.

During the experiments, dust-particles are not homogeneously distributed over the plasma volume and are detected at the boundaries between the plasma bulk and sheaths where they form two dense clouds parallel to the electrodes. Clouds have the shape of a disc. Between the two dust-particle clouds, the plasma is close to a dust-free plasma. Cloud levitation results from the action of various forces on dust-particles:[24,33–36]

- Gravitational force directed downward (toward the grounded electrode).
- Electric force due to the potential gradient within the sheaths and pushing negatively charged dust-particles toward the plasma bulk.
- Thermophoretic force induced by the temperature gradient in the gas and pushing dust-particles toward colder regions of the discharge. As the RF electrode is not cooled and is heated by the bombardment of positive ions accelerated by the negative DC self-bias voltage, this force pushes dust-particles located near the RF electrode toward the grounded one.
- Ion drag force due to the flow of positive ions coming from the plasma bulk toward the electrodes and pushing dust-particles in the same direction.
- Repulsive electrostatic force between negatively charged dust-particles within a cloud.

Grown dust-particles start to levitate in a cloud parallel to the RF electrode and for a while, the different forces are in balance. Dust-particles are trapped as long as the ion drag force that pushes dust-particles toward the RF electrode balances the other forces directed downward: gravity, thermophoresis, and electric forces. After a few minutes, the increase of both dust-particle diameter and RF electrode temperature induces an enhancement of gravity, electric forces, and thermophoresis. The ion drag force is no longer efficient to sustain dust-particles close to the RF electrode. Consequently, dust-particles progressively fall through the plasma bulk and become trapped above the grounded electrode thanks to the electric force present in the bottom sheath vicinity. Finally, when dust-particles are too heavy, they fall onto the grounded electrode. When dust-particles have fallen out of the plasma onto the grounded electrode, no new dust-particles are formed again spontaneously. This global dust-particle dynamics has been previously described by considering the role and evolution of the different forces during the growth process.[24]

IV. RESULTS AND DISCUSSION

The experimental protocol described in Sec. II was carried out several times to obtain reliable results for the comparison between clean and coated electrode conditions.

A. Dust-particle growth and dynamics by LLS

The behavior of the grown dust-particles is made visible by the laser beam directed through the levitation areas. Due to the laser wavelength, it can be assumed that only dust-particles with diameters larger than 50 nm are detected. As the dust-particles are generated and grown, they accumulate in a cloud localized at the RF sheath boundary.

Figure 2 shows images of the dusty plasma at 350 s and 800 s after plasma ignition with initially clean electrodes. Laser light scattering evidences dust-particle cloud (green color) near the biased electrode at 350 s but this cloud has disappeared at 800 s. Moreover, at 800 s, the ion bombardment on the powered electrode leads to the appearance of bigger objects ("coating flakes") that come from the spalling of the coating deposited on the biased electrode during this experimental run. In images, coating flakes are easily distinguished from dust-particles as they appear as rather big luminous points or lines.

Figure 3 presents the time evolution of the dust-particle cloud diameter near the biased electrode. This diameter depends on the dust-particle size and number density. In the plasma, dust-particles start to be detected at about 50 s after the discharge ignition in the clean case and 30 s in the coated one. The dust-particle cloud diameter up to 200 s is larger in the coated case. Dust-particle growth at the beginning of the experiment is faster when there is an initial coating on the biased electrode. The fall of spherical dust-particles trapped in the upper cloud starts about 180 s after the

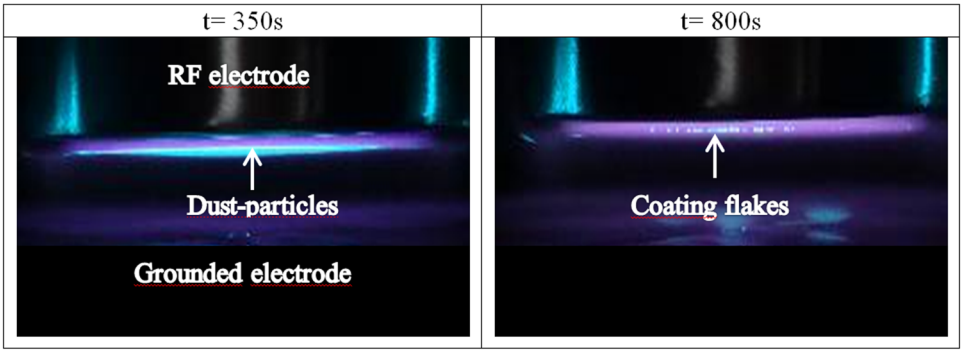

FIG. 2. LLS images in the dust-particle cloud near the biased electrode at two experimental times with initially clean electrodes.

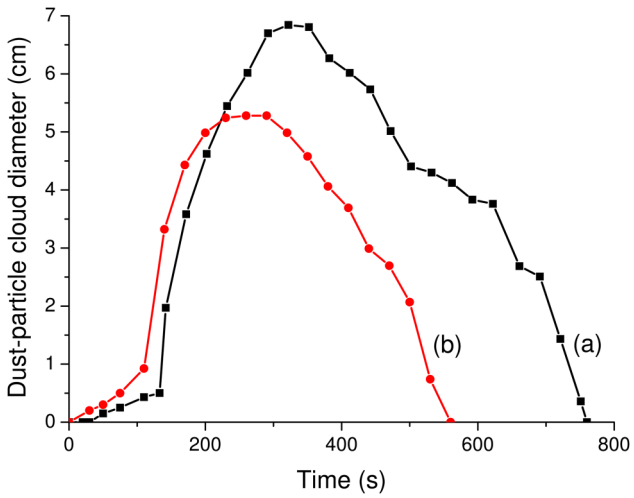

FIG. 3. Time evolution of the diameter of the dust-particle cloud near the biased electrode: (a) clean and (b) coated conditions.

discharge ignition in the coated case and 270 s in the clean one. But as new dust-particles are generated during the next 100 s and as the present dust-particles continue to grow, the cloud diameter slightly increases and reaches a constant value. The maximum diameter, around 6.8 cm, is much larger in clean than in coated conditions, where it is only about 5.3 cm. The number of dust-particles seems to be greater in clean rather than in coated conditions. From about 300 s and 370 s in the coated and clean cases, respectively, no new dust-particles are generated, and the cloud diameter regularly decreases. Approximately 600 s after the plasma ignition, the dust-particle cloud near the biased electrode has partially emptied in the clean case, whereas the dust-particles cannot be detected any longer in the coated case. For both conditions, when this dust-particle cloud has completely disappeared, i.e., for times around 560 s and 800 s to the coated and the clean cases, respectively, only some coating flakes levitate under the biased electrode (Fig. 2) or fall through the plasma. The spalling of the coating on the biased electrode occurs as soon as the discharge is ignited in the coated case while it starts after 360–400 s in clean conditions. This delay in the clean conditions corresponds to the necessary plasma duration to obtain a sufficiently thick coating on the electrode.

To explain the faster growth in the coated case, the origin of dust-particle precursors has to be taken into account. In the clean case, precursors originate from chemical reactions directly in the gas phase, while in the coated case, an additional source of precursors exits. Indeed, the energetic ion bombardment of the RF electrode covered by a hydrocarbon thin film leads to the sputtering of atoms or small molecular fragments.[37] The obtained results suggest that these sputtered species also participate in dust-particle growth and thus accelerate their formation in the coated case.

B. Spherical dust-particles and coating flakes using SEM

At the end of some experiments, dust-particles and coating flakes that have fallen onto the grounded electrode are collected and observed using SEM as shown in Fig. 4. Flakes display a yellow-brown color and are 100 μm long and 10 μm wide, while dust-particles present a spherical shape and display a white color. A more precise SEM analysis of dust-particles is performed in the clean and coated cases as presented in Fig. 5. In both cases, dust-particles are spherical and present either a smooth surface or a cauliflowerlike surface structure according to their size as also observed in the literature.[38] As dust-particles have a regular spherical shape, the measured diameters give an accurate measurement of the size distribution. In each case, the diameters of 300 dust-particles were directly and manually measured from SEM pictures in order to have a good statistic as can be seen in Fig. 6. The diameter distribution of dust-particles is centered at approximately 1.2–1.3 μm (average diameter) whatever the electrode cleanliness conditions. In both cases, the dust-particle diameters range from about 0.9 μm to about 1.7 μm. However, in the coated case, the size dispersion is slightly larger and dust-particles with diameters higher than 1.2 μm are more numerous. This is explained by the fact that two simultaneous precursor origins exist in coated conditions (from the surface and the gas). In addition, as particles appear faster in the coated case, some of them have a larger final size (than in the clean case) 20 min after plasma ignition. Nevertheless, from these analyses, it seems that the deposited hydrocarbon film has very little influence on the final dust-particle size and morphology.

C. DC self-bias voltage measurements

Dust-particles trap electrons from the plasma bulk and become negatively charged. Consequently, the growth and levitation of dust-particles below the RF electrode affect the DC self-bias voltage. Thus, thanks to its time evolution, it is possible to follow the dust-particle growth, the cloud expansion, and their fall through the plasma. It was evidenced in previous works[39–41] for clean conditions that V_{DC} evolution is correlated with the time evolution of laser light scattering and extinction. Figure 7 displays a typical V_{DC} time evolution in

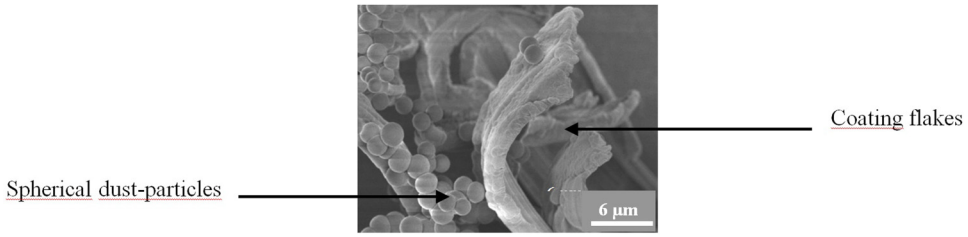

FIG. 4. SEM images of collected spherical dust-particles and coating flakes.

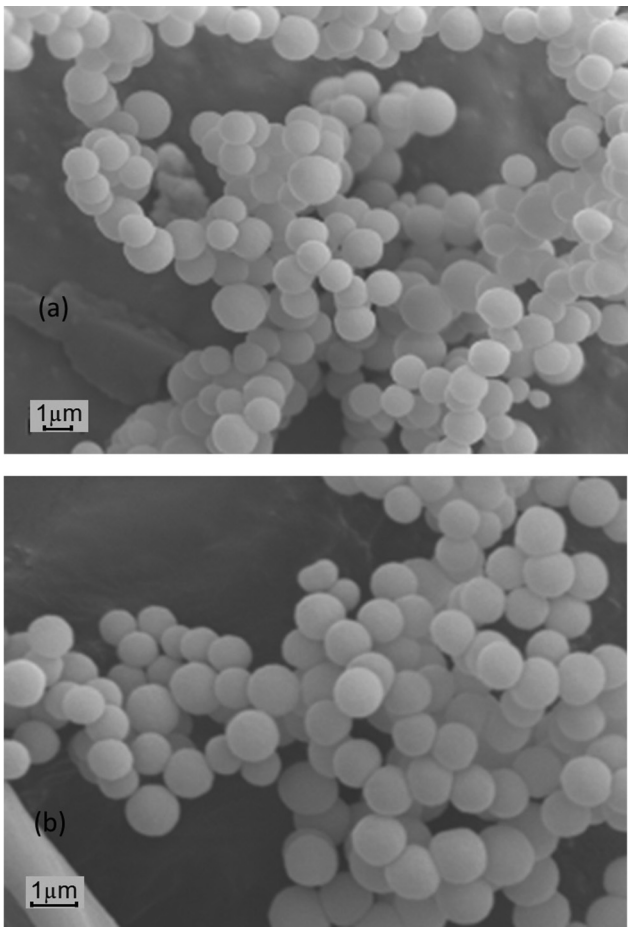

FIG. 5. SEM images of collected spherical dust-particles in (a) clean and (b) coated conditions.

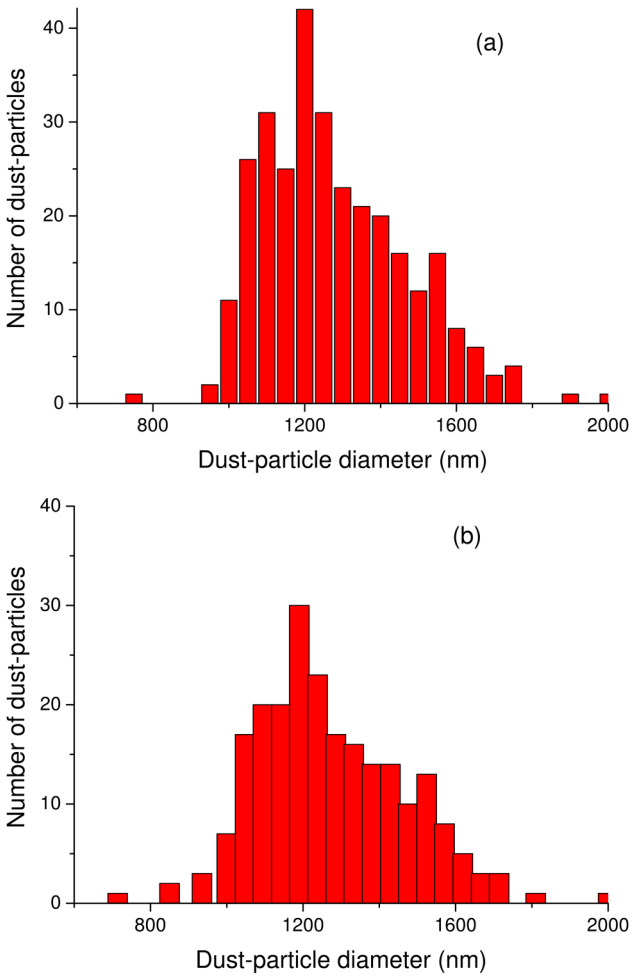

FIG. 6. Size distribution of collected spherical dust-particles in (a) clean and (b) coated conditions.

clean and coated cases. The V_{DC} evolutions can be divided into two phases (1) and (2), separated by a dotted line, to highlight different dust-particle behaviors within the plasma bulk.

First of all, the experiment performed in clean conditions is considered by correlating curve (a) in Figs. 2, 3, and 7. At the beginning of phase (1), V_{DC} increases when electrons are trapped by small growing dust-particles still not visible in Fig. 3 because they are less than 50 nm in diameter. Then, as more and more dust-particles are formed and grown, the dust-particle cloud below the RF electrode expands. The direct consequence is that more and more electrons are trapped by dust-particles: the DC self-bias voltage reaches its maximum value at around 200 s. During this first phase, dust-particles levitate under the RF electrode because forces are balanced. From 200 s to 370 s, the DC self-bias voltage begins to decrease, meaning that fewer electrons are trapped below the RF electrode. Indeed, the gravity, electric, and thermophoretic forces continue to increase and the balance is broken: the heaviest dust-particles (around 1 μm in diameter) start moving downward, the small ones are still growing and some new dust-particles are still created. From 370 s, at the beginning of the phase (2), the slope of the V_{DC} curve is modified: no more small dust-particles are generated and the cloud located below the RF electrode progressively empties (Fig. 3), whereas a dust-particle cloud above the grounded electrode appears and expands. The V_{DC} signal decreases and goes back approximately to its initial value when there are no more spherical dust-particles below the powered electrode; only a few coating flakes accumulate and still levitate below the biased electrode (Fig. 2, t = 800 s).

The correlation between V_{DC} and the dust-particle behavior is roughly similar in the coated case. Nevertheless, evolutions of V_{DC} in the two cases have slight discrepancies as shown in Fig. 7. The initial V_{DC} value (at t = 0 s) varies very slightly from one experiment to another. Its typical value is around −170 V for experiments in clean conditions and −180 V in the coated case. Then, the V_{DC} value gradually becomes less negative: up to −125 V in the clean case and up to −165 V in the coated one. This initial

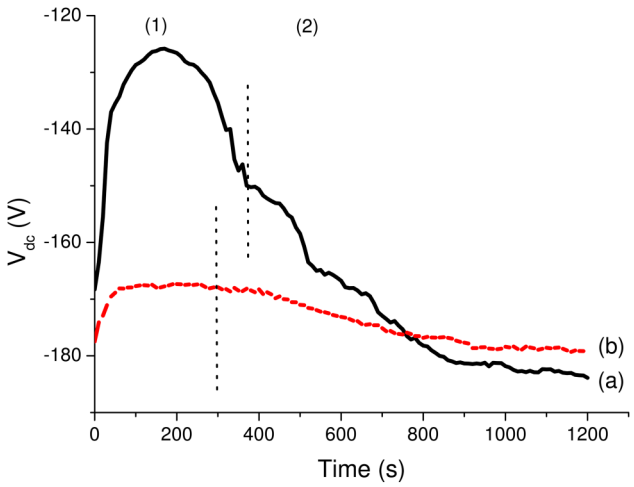

FIG. 7. Time dependence of V_{DC} in (a) clean and (b) coated conditions.

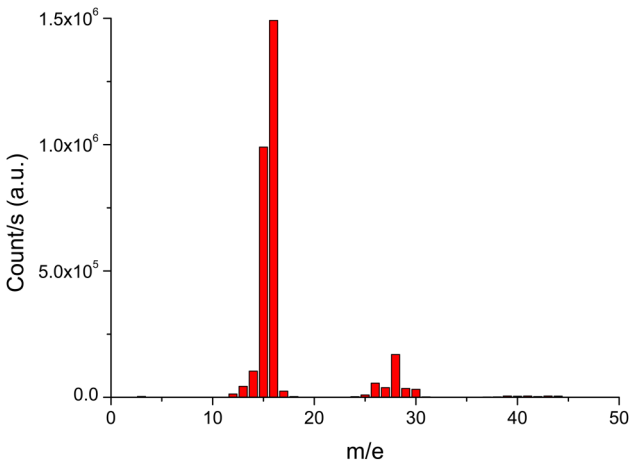

FIG. 8. 0–50 m/e typical mass spectrum of neutral species in clean conditions.

variation in amplitude is much larger in clean conditions, $\Delta V_{DC} = 55$ V, than in coated ones where it is only 15 V. It indicates that in the coated case, fewer electrons are trapped by dust-particles, meaning a less important production of dust-particles and a smaller cloud under the RF electrode (Fig. 3). Moreover, the time corresponding to the maximum value of V_{DC} is about 200 s in clean conditions, while it is only 70 s in the coated case. In the coated case, the maximum value remains rather constant during about 200 s. It means that the dust-particles' appearance is faster with coated electrodes as it was observed by other authors.[42] This is consistent with Fig. 3 showing that during phase (1), the cloud diameter is larger in the coated case.

D. Mass spectrometry

In order to reveal the evolution of the gas phase chemistry during dust-particle growth in CH_4, both neutral and ionic species are analyzed by MS.

1. Neutral species

Figure 8 shows a typical mass spectrum of the neutral species created within the pure CH_4 discharge.

Observed neutral species result not only from the dissociation of CH_4 by electron impact but also from neutral-neutral reactions and ion-molecule reactions.[43] The most abundant neutral species is CH_4 at 16 amu, also being evidenced by m/e peaks at 12–15 amu originated from the fragmentation of the parent molecule. The presence of a "reagent" ion, CH_5 with a peak at m/e = 17,[44] and the production of cracking patterns of neutral species with masses in the range 25–30 amu can also be observed. Mass 26 amu can be attributed to the formation of acetylene C_2H_2 in the plasma and fragmentation of plasma ethylene C_2H_4 in the ionization chamber of the mass spectrometer. For the same reason, mass 28 amu corresponds to both C_2H_4 formed in the plasma and fragmented ethane C_2H_6 molecules, the presence of ethane in the plasma being confirmed by the peak at 30 amu.

During the whole process, the plasma chemistry is analyzed by MS. The time dependence of signals measured at masses 16 (CH_4), 26 (C_2H_2 and C_2H_4), and 28 (C_2H_4 and C_2H_6) amu are represented in Fig. 9 in (a) clean and (b) coated cases. Since it is the precursor gas, CH_4 signal is large prior plasma ignition. The dissociation of CH_4 and thus its consecutive consumption are accompanied by the progressive appearance of new heavy neutral molecules corresponding to various hydrocarbons such as C_2H_2, C_2H_4, C_2H_6, etc.

After the plasma ignition, the methane follows an approximately exponential decay, while the C_2H_x species show a pronounced increase. Similar evolutions were obtained in CH_4/Ar gas mixtures of a dielectric barrier discharge.[45] Over the investigated time range, the C_2H_x concentration first increases (for time $t < 200$ s) and, after achieving a maximum value, it shows a continuous decay. This decrease indicates that C_2H_x molecules probably serve as intermediate steps for the formation of larger hydrocarbons like C_3H_x and C_4H_x. These molecules are detectable at very low concentrations. Their temporal evolution (not shown here due to their low signal to noise ratio) is roughly comparable to C_2H_x species (Fig. 9).

The constant decrease of the initial precursor molecule (CH_4) and the appearance of heavier elements clearly show the beginning of polymerization reaction in the gas phase. The further decrease of all the masses shown in Fig. 9 is the direct consequence of their involvement in chemical reactions that will finally lead to the growth of both spherical dust-particles in the plasma bulk and thin hydrocarbon films on the electrodes.

In present experiments, spherical dust-particles are formed spontaneously, while in the case of many other studies in CH_4 or Ar/CH_4, the nucleation must be initiated externally.[14,15,38,46] Hong *et al.*[38] explained that acetylene (C_2H_2) is the precursor of dust-particle production in CH_4 discharges. Thus, dust-particle

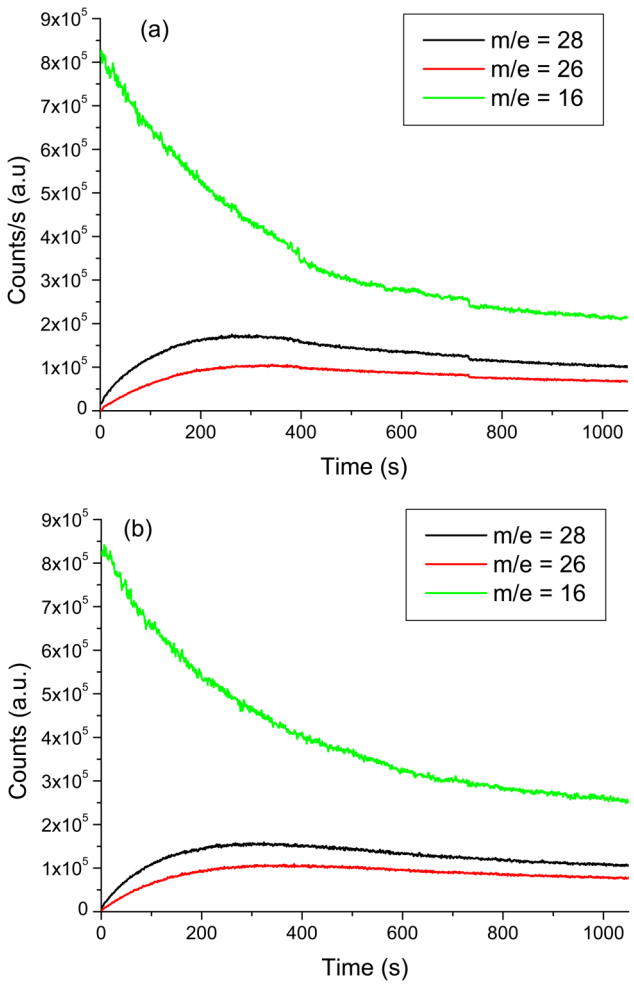

FIG. 9. Time evolution signals corresponding to CH_4 (m/e = 16), C_2H_2 (m/e = 26), and C_2H_4 (m/e = 30) in (a) clean and (b) coated conditions.

generation can be obtained either by applying transient high power to the discharge or by transiently adding a small amount of C_2H_2. In their study, the transient power per unit volume to obtain a dust-particle generation in CH_4 gas is 0.19 W/cm^3. In our case, the constant power per unit volume has a relatively close value, around 0.22 W/cm^3; and this may explain our spontaneous dust-particle generation. In their study, they showed a cyclic production of dust-particles when the discharge is operating in acetylene, whereas a single generation is possible in pure methane as in the present experiments. In their discharge in pure CH_4, or in CH_4 with C_2H_2 injections, MS signals of C_2H_2 and CH_4 decrease during dust-particle growth. In our experimental conditions and whatever the electrode cleanliness at the plasma ignition, the signal of the CH_4 mass also decreases to a steady minimum value during the experiment. On the contrary, the time evolution of C_2H_2 mass is quite different. As soon as the CH_4 is injected into the chamber, a certain amount of C_2H_2 molecules is formed due to chemical reactions in the plasma bulk. This amount of C_2H_2 may be sufficient to initiate the spherical dust-particle generation. Dust-particles are suspended in the plasma near the biased electrode until 560 s for the coated case and 800 s for the clean one (Fig. 3). Nevertheless, even if the upper dust-particle cloud has disappeared, the C_2H_2 concentration remains high enough and should allow the formation of new dust-particles but it is not the case. About 350 s after the beginning of the experiment, the slow decrease of C_2H_2 concentration is an indication of its consumption during dust-particle growth and thin film deposition on the electrodes. So, in the performed experiments, only the presence of C_2H_2 in the plasma does not explain the dust-particle generation.

To summarize, as all mass spectra were taken under similar conditions of pressure and power in the clean and the coated conditions:

- No significant differences are observed in the time evolution of the neutral species.
- Hydrocarbon radicals and neutral species are roughly of comparable importance. Nevertheless, in the clean case, the decrease of CH_4 appears to be stronger and masses 26 and 28 are produced in slightly larger amounts. This is consistent with a larger production of dust-particles as already shown in Figs. 3 and 7.
- In the coated case, the measurements of the cloud diameter show that the dust-particle growth is faster. A hypothesis could be that the sputtered coating provides locally (in the close vicinity of the RF electrode) species involved in dust-particle growth. These localized species cannot be detected by the MS located in a place where it can mainly sample the species produced in volume.

2. Ionic species

Presumably, both positive and negative ions also contribute to the spherical dust-particle growth in the plasma bulk and to the hydrocarbon film growth onto the electrodes. As the negative ions are trapped within the plasma by the plasma potential, it is very difficult to detect them by mass spectrometry. Negative ion mass spectra are usually obtained at the plasma extinction by pulsing the discharge. As the present RF generator is not optimized for working in pulsed mode, only positive ions will be discussed in the rest of this section.

To collect positive ions coming from the plasma, the MS extractor is set to a negative voltage. Then, the energy, for which the maximum ion signal is collected, is used to scan the species in mass. Figure 10 displays a typical mass spectrum of the positive ions in the mass range 0–100 amu.

As for the neutral species, the same positive ionic species were observed in the clean and coated conditions. Primary ions CH_3^+ and CH_4^+ produced by electron impact ionization of methane in the plasma are observed. Secondary ions such as CH_5^+ (17 amu), $C_2H_5^+$ (29 amu), $C_3H_7^+$ (43 amu), $C_4H_7^+$ (55 amu), $C_5H_7^+$ (67 amu), $C_6H_{11}^+$ (83 amu), and $C_7H_{11}^+$ (95 amu), produced through ion-molecule reactions are also observed in relatively high proportions.

The CH_5^+ and $C_2H_5^+$ ions are practically all formed through ion-molecule reactions with reaction-rate coefficients are of the

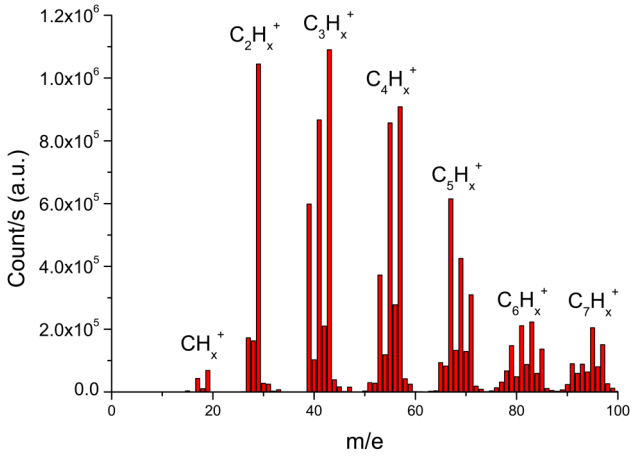

FIG. 10. 0–100 m/e typical mass spectrum of positive ions in clean conditions.

order of 10^{-9} cm^3/s[44]

$$CH_4^+ + CH_4 \rightarrow CH_5^+ + CH_3,$$

$$CH_3^+ + CH_4 \rightarrow C_2H_5^+ + H_2.$$

Under the studied plasma conditions, it should be noted that the $C_3H_7^+$ ion is one of the ions which is easily created in the plasma. Ion-neutral reactions lead to the formation of heavy hydrocarbon positive ions as can be seen in the following reactions:

$$C_2H_5^+ + CH_4 \rightarrow C_3H_7^+ + H_2,$$

$$C_2H_5^+ + C_2H_4 \rightarrow C_3H_5^+ + CH_4,$$

$$C_2H_5^+ + C_2H_4 \rightarrow C_4H_9^+.$$

At this stage, no clear difference in the detected ions is observed between the clean and coated conditions. In order to reveal possible differences in the positive ion population, their energy is now analyzed in detail.

3. Energy of ionic species

For the two cases of the experimental protocol, Fig. 11 gives an example of the energy distribution of different positive ions 20 min after the plasma ignition when there are no more dust-particles.

The full width at half maximum of the energy is somewhat dependent on the m/e values of the ions ranging from 2 to 4 eV. The maximum value of the energy is connected to the plasma potential.[47,48] The energy distribution for all positive ionic species displays a single energy peak with a pronounced maximum around 22 eV and 30 eV for experiments carried out in clean and coated conditions, respectively. In order to confirm values obtained for the plasma potential (V_p), a heated Langmuir probe has been used in the clean case, the heating being used to reduce thin film deposition on the probe surface. The plasma potential was determined

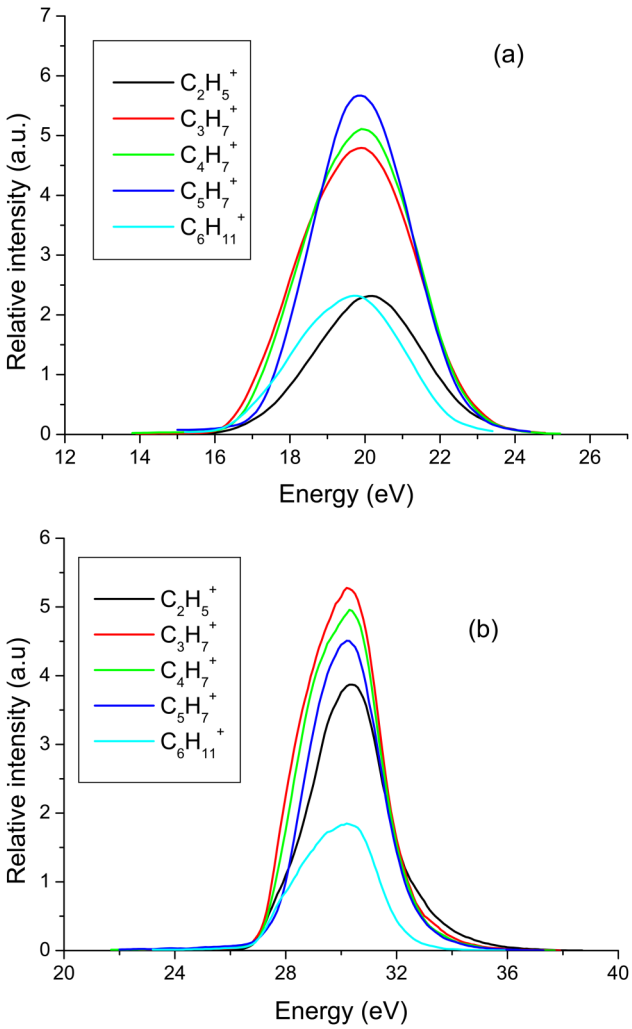

FIG. 11. Energy distribution of positive ions of different masses in (a) clean and (b) coated conditions.

from the maximum of the derivative curve of I(V) characteristics. This intrusive method[49] gives a rough estimation of the plasma potential at the end of the clean experiment around 25 V close to the values measured by MS. The correlation between these two measurements allows to be relatively confident on the determination of the plasma potential. Figure 12 displays the time evolution of the $C_2H_5^+$ mean ion energy in clean and coated conditions.

In the clean case, the energy increases up to 52 eV and then decreases regularly reaching a value around 22 eV. In the same way, the measured plasma potential using the Langmuir probe ranges typically from 60 to 25 V. In the coated case, the energy regularly and slowly decreases from 36 eV at the beginning of the experiment to 30 eV at the end. The ion energy variation during the experiment is much larger in clean conditions, around 30 eV, than in coated ones where it is only about 6 eV. From the beginning of

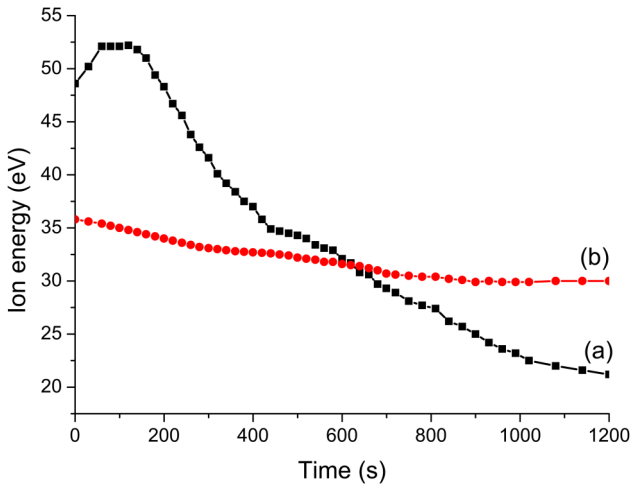

FIG. 12. Temporal evolution of the positive ion $C_2H_5^+$ energy in (a) clean and (b) coated conditions.

the experiment up to 200 s, dust-particles progressively and spontaneously appear and grow, and they attach free plasma electrons. As the plasma loses electrons, its potential tends to increase to limit this loss and that is why both ion energy and V_{DC} increase at the beginning. Then, due to the dust-particle dynamics, some of them start to be lost or to fall closer to the grounded bottom electrode. The loss of free electrons is reduced and the ion energy decreases progressively. The increase at the beginning is much less pronounced in the coated case due to the fact that fewer dust-particles are produced and thus the plasma is not changing so much (such as V_{DC}). In the range 200–370 s, as was mentioned in Sec. IV C, fewer electrons are trapped by dust-particles, so the ion energy and V_{DC} curves strongly decrease. For times between 370 and 800 s, the slope of the curves changes and becomes smaller because there are fewer and fewer dust-particles under the biased electrode. Finally, after 800 s, both ion energy and V_{DC} tend toward constant values because there are no more dust-particles and no more electrons are trapped. In the coated case, at the beginning of the experiment, the ion energy does not follow the evolutions of both V_{DC}. After the plasma ignition, dust-particles quickly grow (Fig. 3) but their production is less important than in the clean case. Dust-particle appearance is accompanied by a smaller electron trapping, a smaller V_{DC} variation, and a smaller ion energy value. At the beginning of the experiment, the electron trapping is not sufficiently high to provide a significant ion energy increase as it was shown in the clean case. Then, the regular decrease of the ion energy is consistent with the clean case when dust-particles leave the cloud under the biased electrode (for time ranging from 300 s to 560 s). Finally, the ion energy value at the end of the experiment is larger in the coated case than in the clean one (Fig. 11). The spalling of the coating on the biased electrode leads to the sputtering of flakes that stay trapped near the biased electrode or fall through the plasma. We assume that the flakes are negatively charged before falling on the grounded electrode. As in the coated case there are more flakes in the plasma, more electrons are trapped explaining the larger ion energy. However, we specified also at the end of Sec. IV D 1 that the mass spectrometer is in a place where it can reflect only important changes in the plasma volume, and it explains why the evolution of the measured ion energy does not reflect perfectly all the changes observed in V_{DC}.

The sputtering of the electrodes by the ion bombardment seems to play a significant role in the dust-particle growth in our experiments. The ion bombardment depends among other parameters on the energy of ions when they strike the electrodes. Positive ions created in the plasma glow are accelerated toward both electrodes with average energy depending on the difference between the plasma potential and the electrode potential. Positive ions striking the grounded electrode have the energy directly fixed by the plasma potential while those striking the powered electrode acquire an average energy close to the difference between V_{DC} and the plasma potential. This energy is calculated from the experimentally measured V_{DC} and from the determined V_p using the MS results. To distinguish the ion energy measured by mass spectrometry and the ion energy acquired in the RF sheath, we will call this last one "striking energy of ion." Looking at the time evolution of the "striking energy of ions" in Fig. 13, one can see that positive ions striking the powered electrode acquire a smaller energy in the clean case (in the range 175–215 eV) than in the coated one (200–215 eV).

Figure 13 is directly connected to explanations of Figs. 3, 7, and 12. In both cases, it evolves during dust-particle trapping under the biased electrode according to V_{DC}. The sputtering of the RF electrode is more significant in the coated case, and a higher number of atoms or molecular fragments are ejected. The precursor number for the dust-particle growth is also more important, so the dust-particle growth is quicker. At the end of the experiment when there are no dust-particles under the biased electrode, after around 800 s, the "striking energies of ions" are slightly close, showing that the influence of the pollution state of the biased electrode is almost

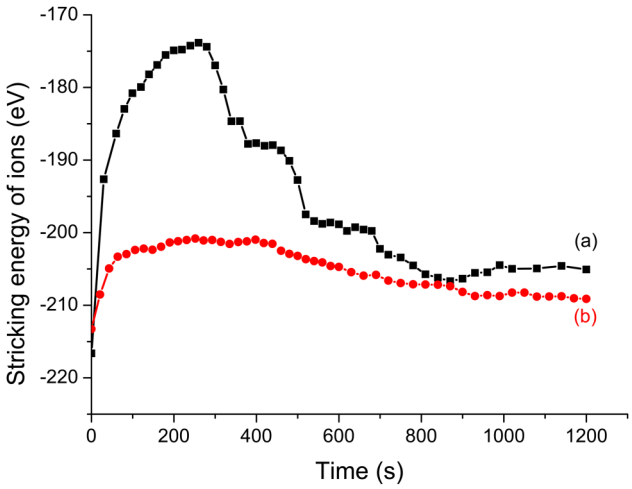

FIG. 13. Temporal evolution of the average energy of positive ions striking the powered electrode: (a) clean and (b) coated conditions.

the same in the clean and in the coated case. It also confirms the assumption concerning the fact that the higher ion energy at the end of the experiment comes from the electron trapping by the flakes. Finally, in the coated case, the earlier falling of the dust-particles (Fig. 3) due to the higher electric force pushing the dust-particles downward is connected to the higher voltage drop between the plasma and the RF electrode.

4. $C_2H_5^+$ and $C_3H_7^+$ ions

At this point, it is necessary to make an assessment of the relative amounts of positive ions in the two cases. For that, the relative contributions of $C_2H_5^+$ and $C_3H_7^+$ are analyzed (Fig. 14).

For each energy profile (such as in Fig. 11), the underneath area is calculated. Therefore, the obtained values are roughly connected to the relative number of positive ions in the plasma. For simplicity's sake, in the following, we will call "ion number" the underneath area.

Looking at the time evolution of the positive ion number, one can see that positive ions have almost the same evolution in experiments performed in clean and coated conditions. At the beginning of the experiments, $C_2H_5^+$ and $C_3H_7^+$ ion numbers are higher in the clean case. The decrease of $C_2H_5^+$ and $C_3H_7^+$ ion number until 100–200 s after the plasma ignition, in both conditions, can be correlated to the increase of the V_{DC} curves (Fig. 7) and so to the dust-particle growth. In the range 200–370 s, the positive ion number stays almost constant, suggesting a balance between their formation and their consumption during the dust-particle growth. Then, for times greater than 370 s, the dust-particle cloud near the biased electrode continuously empties and feeds the dust-particle cloud near the grounded electrode, leading to a regular increase of the ion number until the end of the experiment. For both experiments, the signal corresponding to $C_3H_7^+$ ions is slightly larger than the one for $C_2H_5^+$ ions except at the very first beginning.

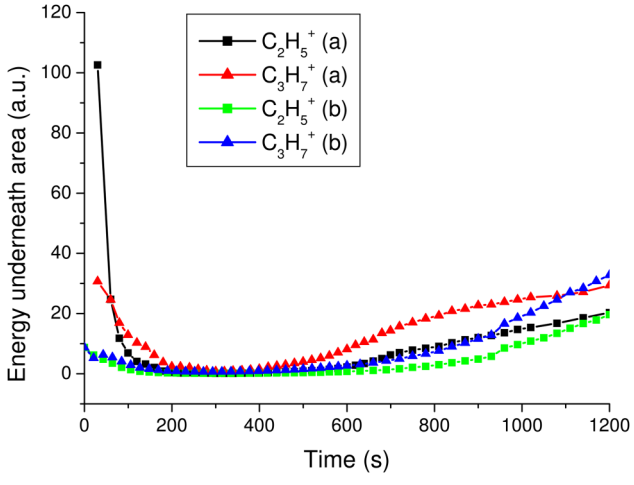

FIG. 14. Comparison of the temporal evolution for $C_2H_5^+$ and $C_3H_7^+$ ions in (a) clean and (b) coated conditions.

The methane dissociation and the different chemical reactions lead to a continuous formation of positive ions of increasing mass. The simultaneous fragmentation and recombination of lightweight ions (such as $C_2H_5^+$) as well as their participation in the coating growth could explain their smaller increase in the plasma after 500 s.

It is well known that the surfaces confining a plasma play an important role in plasma chemistry.[50,51] According to Sobolewski,[52] the electrode surface is an important parameter in the reproducibility of the discharges. The surface chemistry depends on the surface properties (material, structure, etc.) and on the energy and type of incoming particles. These electrode surfaces, bombarded by ions from the plasma, can emit secondary electrons. One of the parameters that changes in the present experiments is the surface state of the aluminum electrode: at the beginning of the experiment, it is either film-free or covered by a thin hydrocarbon film. Stefanovic *et al.*[53] showed that the secondary electron emission yield is higher for a clean stainless-steel electrode than for an electrode covered by a hydrocarbon film. Taking into account these studies, we assume that in clean conditions, this larger secondary electron emission induces a better ionization in the plasma bulk and could explain the larger number of positive ions at the beginning of the experiment than in coated case. On the other hand, we can assume that the faster growth of dust-particles in the coated case could lead to a more important consumption of ions by dust-particles.

E. Concluding remarks

Results obtained in this study show that the cleanliness of the reactor plays a significant role in the dust-particle production. Experiments are carried out in two different initial conditions for the electrodes: without any coating or with a homogeneous hydrocarbon coating.

Dust-particle generation requires the presence of precursors in the plasma. These precursors result from two phenomena occurring simultaneously:

1. Dust-particle precursors could originate from the plasma chemistry in the gas phase. Plasma electrical parameters are in constant evolution, so they have an influence on the precursor appearance and on the dust-particle growth.[54]
2. Dust-particle precursors could also originate from the sputtering of the coating on the biased electrode. Sputtered atoms and molecules will participate to the plasma chemistry and to the dust-particle formation and growth.

However, in our experiments, one may wonder why time needed to make precursors would be shorter in the coated case and which phenomena are responsible for the dust-particle growth?

In the case of a film-free electrode at the beginning of the experiment, the coating is growing on the biased electrode as the discharge is on. In the coated case, the initial hydrocarbon film on the RF electrode and the higher "striking energy of ions" induce a more important and more effective sputtering. With this energetic ion bombardment, changes in the surface material are induced: (i) on one hand, new chemical bonds can be formed between incident ions and the growing layer; (ii) on the other hand, atoms, molecules, small molecular fragments, and coating flakes can be ejected from the growing layer by sputtering.

In the clean and the coated cases, the dust-particle generation starts from the beginning of the experiments as shown in the time evolutions of the V_{DC} and the ion energy. However, the detection of the dust-particles by LLS in the coated case shows that the dust-particles appear earlier. Indeed, as both precursors coming from the gas phase and from the sputtering of the RF electrode are present at the beginning of the experiment, the dust-particle growth is faster than that in the clean case. We suggest that in clean conditions, even if the dust-particles are generated at the beginning of the experiment, an enough coating thickness of the coating on the biased electrode is necessary to speed up their growth. Nevertheless, the two phenomena leading to the dust-particle precursors occur simultaneously and are inseparably associated with each other.

Besides the different physical and chemical processes leading to the dust-particle formation, the RF electrode cleanliness and its sputtering play a crucial role in dust-particle growth.

V. CONCLUSION

The dusty plasma chemistry and the dust-particle growth were compared in two kinds of experiments with different electrode surface states at the plasma ignition: (i) clean (without any film) and (ii) with a homogeneous hydrocarbon coating. The various neutral and ionic species involved in the dust-particle formation and growth are revealed by time resolved mass spectrometry. Neutral species are not clearly affected by the surface state of the biased electrode whereas the number of positive ionic species and their energy are affected. First, positive ions are consumed for dust-particle and coating growth. Once dust-particles are leaving the vicinity of the biased electrode, the number of positive ions regularly increases. It is also shown that the temporal evolution of both the average positive ion energy and the "striking energy of ions" are affected by the electrode cleanliness. During an experiment, positive ions striking the biased electrode acquired a higher energy in coated than in clean conditions. As a consequence, dust-particle formation in CH_4 plasmas might be partly induced by plasma-surface interactions, e.g., sputtering or etching processes, leading to the formation of dust-particle precursors. Thus, dust-particles grow faster in coated than in clean conditions.

In order to reveal the role of molecules sputtered from the coating, further works will be oriented to analyze and compare the chemical composition of both dust-particles and hydrocarbon coatings in the two experimental conditions.

ACKNOWLEDGMENTS

The authors would like to thank J. F. Lagrange for helpful discussion and the "Institut Universitaire de Technologie" of Bourges (France) for scanning electron microscopy analyses. They also thank the "Région Centre Val de Loire," the "Conseil Départemental du Cher" and the European community via FEDER contract for the mass spectrometry device (Inventory No. 308B 02).

REFERENCES

[1]I. Langmuir, C. G. Found, and A. F. Dittmer, Science **60**, 392 (1924).
[2]G. S. Selwyn, J. Singh, and R. S. Bennett, J. Vac. Sci. Technol. A **7**, 2758–2765 (1989).
[3]M. M. Smadi, G. Y. Kong, R. N. Carlile, and S. E. Beck, J. Vac. Sci. Technol. B **10**, 30 (1992).
[4]K. Nishioka, S. Horita, K. Ohdaira, and H. Matsumura, Sol. Energy Mater. Sol. Cells **92**, 919 (2008).
[5]K. Nishioka, T. Sueto, and N. Saito, Appl. Surf. Sci. **255**, 9504 (2009).
[6]C. D. Pintassilgo and J. Loureiro, Adv. Space Res. **46**, 657 (2010).
[7]C. Szopa, G. Cernogora, L. Boufendi, J. J. Correia, and P. Coll, Planet. Space Sci. **54**, 394–404 (2006).
[8]C. J. Mitchell, M. Horányi, O. Havnes, and C. C. Porco, Science **311**, 1587 (2006).
[9]C. Arnas, A. Michau, G. Lombardi, L. Couëdel, and K. Kumar K, Phys. Plasmas **20**, 013705 (2013).
[10]J. Beckers, W. W. Stoffels, and G. M. W. Kroesen, J. Phys. D Appl. Phys. **42**, 155206 (2009).
[11]M. Mikikian, L. Couëdel, M. Cavarroc, Y. Tessier, and L. Boufendi, New J. Phys. **9**, 268 (2007).
[12]M. Mikikian, H. Tawidian, and T. Lecas, Phys. Rev. Lett. **109**, 245007 (2012).
[13]J. Beckers and G. M. W. Kroesen, Appl. Phys. Lett. **99**, 181503 (2011).
[14]C. Deschenaux, A. Affolter, D. Magni, C. Hollenstein, and P. Fayet, J. Phys. D Appl. Phys. **32**, 1876 (1999).
[15]H. T. Do, G. Thieme, M. Fröhlich, H. Kersten, and R. Hippler, Contrib. Plasm. Phys. **45**, 378 (2005).
[16]F. J. Gordillo-Vazquez, M. Camero, and C. Gamez-Aleixandre, Plasma Sources Sci. Technol. **15**, 42 (2006).
[17]S. Hong, J. Berndt, and J. Winter, Surf. Coat. Technol. **174–175**, 754 (2003).
[18]E. Kovacevic, I. Stefanovic, J. Berndt, and J. Winter, J. Appl. Phys. **93**, 2924 (2003).
[19]J. Pereira, I. Géraud-Grenier, V. Massereau-Guilbaud, A. Plain, and V. Fernandez, Surf. Coat. Technol. **200**, 6414 (2006).
[20]M. Hundt, P. Sadler, I. Levchenko, M. Wolter, H. Kersten, and K. Ostrikov, J. Appl. Phys. **109**, 123305 (2011).
[21]G. Al Makdessi, X. Glad, S. Dap, M. Rojo, R. Clergereaux, and J. Margot, J. Phys. D Appl. Phys. **50**, 155203 (2017).
[22]B. Despax, F. Gaboriau, H. Caquineau, and K. Makasheva, AIP Adv. **6**, 105111 (2016).
[23]V. Massereau-Guilbaud, J. Pereira, I. Géraud-Grenier, and A. Plain, J. Appl. Phys. **106**, 113305 (2009).
[24]I. Géraud-Grenier, V. Massereau-Guilbaud, and A. Plain, Eur. Phys. J. Appl. Phys. **8**, 53 (1999).
[25]B. Chapman, *Glow Discharge Processes* (Wiley, New York, 1980).
[26]K. De Bleecker, A. Bogaerts, and W. Goedheer, Phys. Rev. E **73**, 026405 (2006).
[27]A. Bouchoule and L. Boufendi, Plasma Sources Sci. Technol. **2**, 204 (1993).
[28]A. Michau, C. Arnas, G. Lombardi, X. Bonnin, and K. Hassouni, Plasma Sources Sci. Technol. **25**, 015019 (2016).
[29]A. Bouchoule, *Dusty Plasma Physics, Chemistry and Technological Impacts in Plasma Processing* (John Wiley & Sons, Singapore, 1999).
[30]S. V. Vladimirov, K. Ostrikov, and A. A. Samarian, *Physics and Applications of Complex Plasmas* (Imperial College Press, London, 2005).
[31]Y. A. Mankelevich, M. A. Olevanov, and T. V. Rakhimova, Plasma Sources Sci. Technol. **17**, 015013 (2008).
[32]B. P. Pandey, A. Samarian, and S. V. Vladimirov, Phys. Plasmas **14**, 093703 (2007).
[33]O. Havnes, T. Nitter, V. Tsytovich, G. E. Morfill, and T. Hartquist, Plasma Sources Sci. Technol. **3**, 448 (1994).
[34]A. Barkan and R. L. Merlino, Phys. Plasma **2**, 3261 (1995).
[35]L. Couëdel, M. Mikikian, L. Boufendi, and A. A. Samarian, Phys. Rev. E **74**, 026403 (2006).
[36]J. Perrin, P. Molinas-Mata, and P. Belenguer, J. Phys. D Appl. Phys. **27**, 2499 (1994).
[37]J. Benedikt, J. Phys. D Appl. Phys. **43**, 043001 (2010).

[38]S. Hong, J. Berndt, and J. Winter, Plasma Sources Sci. Technol. **12**, 46 (2003).
[39]I. Géraud-Grenier, V. Massereau-Guilbaud, and A. Plain, Eur. Phys. J. Appl. Phys. **14**, 187 (2001).
[40]J. Pereira, V. Massereau-Guilbaud, I. Géraud-Grenier, and A. Plain, J. Appl. Phys. **103**, 033301 (2008).
[41]V. Massereau-Guilbaud, I. Géraud-Grenier, and A. Plain, Eur. Phys. J. Appl. Phys. **11**, 71 (2000).
[42]C. Hollenstein, Plasma Phys. Control. Fusion **42**, R93 (2000).
[43]N. Mutsukura, S. Inoue, and Y. Machi, J. Appl. Phys. **72**, 43 (1992).
[44]F. W. McLafferty and F. Turecek, *Interpretation of Mass Spectra*, 4th ed. (University Science Books, Mill Valley, CA, 1993).
[45]A. Majumbar, J. F. Behnke, R. Hippler, K. Matyash, and R. Schneider, J. Phys. Chem. A **109**, 9371 (2005).
[46]J. Winter, J. Berndt, S.-H. Hong, E. Kovacevic, I. Stefanovic, and O. Stepanovic, Plasma Sources Sci. Technol. **18**, 034010 (2009).
[47]Y. Feurprier, C. Cardinaud, B. Grolleau, and G. Turban, Plasma Sources Sci. Technol. **6**, 561 (1997).
[48]G. J. Vandantop, M. Kawasaki, R. M. Nix, I. G. Brown, M. Salmeron, and G. A. Somorjai, Phys. Rev. B **41**, 3200 (1990).
[49]N. Bilik, R. Anthony, B. A. Merritt, E. S. Aydil, and U. R. Kortshagen, J. Phys. D Appl. Phys. **48**, 105204 (2015).
[50]B. Sikimic, I. Stefanovic, I. B. Denysenko, J. Winter, and N. Sadeghi, Plasma Sources Sci. Technol. **23**, 025010 (2014).
[51]I. Denysenko, I. Stefanovic, B. Sikimic, J. Winter, N. Azarenkov, and N. Sadeghi, J. Phys. D Appl. Phys. **44**, 205204 (2011).
[52]M. A. Sobolewski, Res. Natl. Inst. Stand. Technol. **100**, 341 (1995).
[53]I. Stefanovic, J. Berndt, D. Maric, V. Samara, M. Radmilovic-Radjenovic, Z. L. Petrovic, E. Kovacevic, and J. Winter, Phys. Rev. E **74**, 026406 (2006).
[54]M. Mikikian, M. Cavarroc, L. Couëdel, Y. Tessier, and L. Boufendi, Pure Appl. Chem. **82**, 1273 (2010).